Braz J Phys (2014) 44:240–246
DOI 10.1007/s13538-013-0175-5

GENERAL AND APPLIED PHYSICS

Influence of Liquid Medium on Optical Characteristics of the Si Nanoparticles Prepared by Submerged Electrical Spark Discharge

Mehdi Mardanian · Nikolai V. Tarasenko · Alena A. Nevar

Received: 18 May 2013 / Published online: 21 April 2014

Abstract We have measured the size, structure, and optical properties for two sets of nanoparticles synthesized via electrical-spark discharge between two plane silicon electrodes immersed in deionized water (DI) and 97 % ethanol. The nanoparticles were characterized by X-ray diffraction (XRD), ultraviolet (UV)-visible absorption spectrometry, Raman spectrometry, transmission electron microscopy (TEM), and Fourier transform infrared spectroscopy (FTIR). The size and optical features of the nanoparticles were studied as functions of nature of the liquid. Nearly spherical, single-crystal, and morphologically similar Si nanoparticles with diameters in the 3–8 and 6–13 nm ranges were formed in the colloidal solutions of water and ethanol, with estimated indirect bandgaps of approximately 1.5 and 1.3 eV, respectively. In both cases, the Raman peaks were blue shifted with respect to those of bulk silicon, a result consistent with the small diameters of the particles. The silicon nanoparticles synthesized in water exhibited strong emission in the violet-blue range, with a double peak near 417 and 439 nm. For those synthesized in ethanol, blue-green emission centered at 463 nm was detected.

Keywords Silicon nanoparticles · Synthesis · Electrical spark discharge · Liquid media

M. Mardanian (✉) · N. V. Tarasenko · A. A. Nevar
Laboratory of Laser Diagnostic of Plasma, B. I. Stefano Institute of Physics, National Academy of Sciences of Belarus, Nezalezhnasti Ave. 70, Minsk 220072, Belarus
e-mail: ma_mardanian@yahoo.com

M. Mardanian
Department of Basic Sciences, Qazvin Branch, Islamic Azad University, Nokhbegan Blv., Qazvin, Iran

1 Introduction

Semiconductor nanostructures exhibit novel interesting features, in particular the visible photoluminescence (PL) that has motivated intense research with a view to nanotechnological applications. In recent years, silicon nanoparticles (Si-NPs) have attracted much attention due to the unique combination of their size-dependent optoelectronic properties and their biocompatibility, which are expected to find a wide range of applications in photonics [1, 2], electronics [3], nanobiotechnology [4], and medicine [5]. There is interest in the properties, fabrication procedures, applications, and characterization of Si nanocrystals.

Semiconductors with indirect band gap are inconvenient for light-emitting devices because they interact weakly with photons. Although silicon constitutes no exception, remarkable luminescence can be observed in this material when the grain size decreases to the nanoscale dominated by quantum-confinement effects. Examples are the visible emissions from porous silicon, which has attracted extensive attention in the last decade, and from Si-NPs. The numerous reports on Si-NP fabrication in the literature cover various methods, such as electrochemical etching [3], chemical route [6], and pulse laser ablation [7–12]. Among these, the chemical route has attracted more attention because it offers simultaneous control over particle size and surface properties, two features of capital importance in nanoparticle functionalization. However, this approach has the drawbacks of demanding chemical products and reducing agents [13, 14] or requiring multistep procedures for the NP size control.

Alternative, easily implementable techniques free from these inconveniences are therefore desirable. The electrical discharge method in liquid environment (EDL) has recently emerged as one such alternative. EDL generates pure nanoparticle colloidal solutions in a simple experimental setup that needs no vacuum equipment, introduces small impurity

concentrations and comprises few production steps. The result is a cost-effective procedure with high nanoparticle yield [15–18]. The synthesis can be carried out in water or in a biocompatible ligand solution, a key to the subsequent successful functionalization of the resulting nanostructures [19]. EDL is similar to laser ablation in liquids (LAL). Studies in the literature show that Si-NPs can be produced by laser ablation of silicon wafer in different liquid media. Few, however, are the papers describing the synthesis of Si-NPs in solution plasmas [17, 18]. Here, we report the preparation of nearly spherical Si-NPs by spark discharge between bulk silicon electrodes immersed in deionized water and pure ethanol. To our knowledge, the synthesis of Si-NPs based on electrical spark discharge of Si electrodes immersed in water and ethanol has never been reported. We studied the microstructure, size distribution, and optical properties of the resulting Si-NPs and show that the liquid medium affects the size and optical features of the resulting nanoparticles.

2 Experimental Section

Figure 1 schematically shows the three main components of the experimental setup designed to fabricate Si-NPs: power supply system, chilling loop, and reactor vessel (glass beaker) with an anode and a cathode inside. A spark discharge was ignited in 150 ml of liquid medium (deionized water or pure ethanol) between two electrodes immersed to a depth of 3 cm. The silicon plates served as electrodes. The electrodes were kept at an optimized separation, approximately 1 mm, to insure a stable discharge. The power supply provided an alternating current (ac) spark discharge with a repetition rate of 100 Hz. The peak current of the pulsed spark discharge was 60 A with a pulse duration of 30 μs. The electrical discharge was initiated by an applied high-frequency voltage of 8.5 kV. During the discharge, a bluish radiation and bubbles containing the evaporated material from the electrodes and products of water and/or ethanol dissociation were observed between the electrodes. Small particles were formed by condensation of the Si vapor coming out of the melting electrode surfaces in the surrounding liquid. The solution became less transparent during the discharge. The discharge was somewhat more stable in water than in ethanol. In the former liquid, we kept stable discharges for 1 min intervals. When this period was extended to 10 min, the solution color became gray violet in deionized water, and dark gray in ethanol. Most of the synthesized products were obtained as suspended powders.

Electrical discharge in liquid media is a simple, convenient procedure to prepare Si-NPs in colloidal solution. The rate of production of Si-NPs in ethanol is larger than in water. For instance, under the aforementioned conditions, the rates in water and ethanol are 40 and 46 mg/h, respectively. After pre-sedimentation for roughly 30 min, solid deposits sunk to the bottom of the vessel. To separate the transparent solution in the upper part of the vessel from the obtained sediment, the discharge-treated liquid, except the last 10 ml and sediment, was carefully poured on a Petri dish. Small quantities of liquid were removed with a pipette from the dish to allow characterization of the synthesized nanoparticles. X-ray diffraction (XRD) patterns were measured in an X-ray diffractometer (D8-Advance, Germany) using Cu–Kα radiation in the 20°–100° 2θ range. Ultraviolet (UV)-visible spectra of the samples were recorded in the spectral 200–800 nm region with a Carry 500 spectrophotometer. The particle size and morphology were investigated by transmission electron microscopy (TEM), with a LEO 906E (Germany) microscope under an accelerating voltage of 120 kV. The samples were prepared for TEM measurements by dropping the solution onto a copper grid coated with an amorphous carbon film and letting it dry in air. Fourier transform infrared (FTIR) spectroscopy provided information on the surface properties of the synthesized Si-NPs. IR reflection spectra of the Si-NPs were recorded on a Nexus Fourier spectrometer. The reflection–absorption (R-A) signals were recorded for 20° incidence on the sample. For Raman spectroscopy, a droplet of the solution was drawn on an Al-coated glass plate. Microprobe Raman spectra of the Si-NPs were recorded by a Raman spectrometer Spectra Pro 500i, operated with a 532 nm Nd-YAG laser (30 mW power) in the backscattering configuration with spectral resolution of about 1 cm^{-1}. PL spectra were measured at room temperature by a SFL 1211A spectrometer with an Xe lamp as an excitation source.

3 Results and Discussion

Figure 2a and b displays the XRD patterns of samples synthesized in water and ethanol, respectively. The peaks are rather sharp, even though the diffractograms were only meant to determine the phase composition of the synthesized powders and were hence obtained from the formed powders after the colloidal solution dried, i. e., from particles that were not sorted by size and may well have been clustered. The main diffraction peaks correspond to the lattice planes of cubic structured silicon (JCPDS No: 40-1487). No amorphous-silicon pattern is observed in XRD. In Fig. 2a, the small peaks hardly distinguishable around 14°, 21°, 30°, and 42° are assigned to the SiO_2 amorphous phase, which the spark discharge in water can generate. Not surprisingly, the Si-NPs grown in water cannot be free from the native oxide. By contrast, no such peaks are seen in the diffractograms from the samples synthesized in ethanol.

In order to better understand the size distribution and the crystalline structure of the Si-NPs, we resorted to TEM. In Fig. 3, the Si-NPs are the dark circles that contrast with the bright background. The image, which offers no evidence of aggregation, shows silicon nanocrystals generated in water

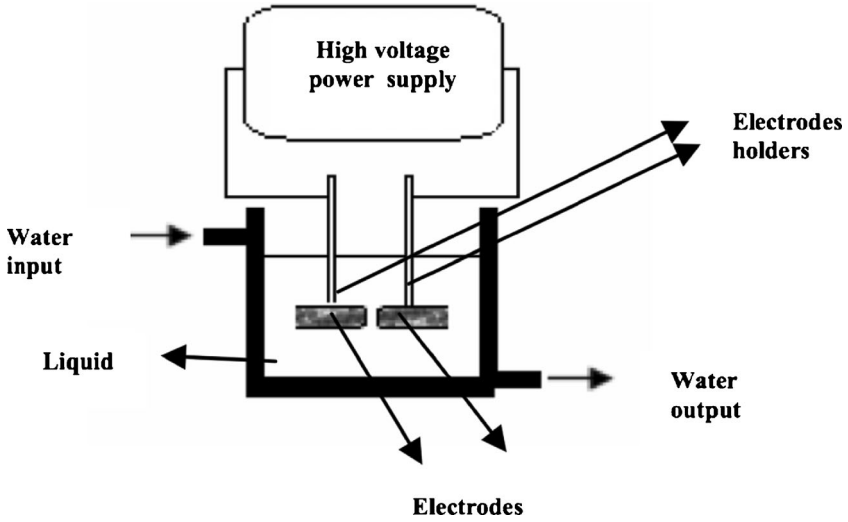

Fig. 1 Schematic diagram of the setup for nanoparticles synthesis by spark discharge in liquids

and ethanol that are approximately spherical, monodisperse, and similar in morphology. Electrical discharges in different liquid media can yield Si-NPs with different size distributions. The typical size distributions of the synthesized Si-NPs were determined by measuring more than 160 particles located at different regions of the grid, as indicated by the histogram on the right-hand side of each image. The sizes of the Si-NPs obtained in water, and ethanol are nearly in the 3–8 and 6–13 nm ranges, respectively. The histograms in Fig. 3 also give a mean diameter of 5 and 9 nm with very small standard deviations of 0.2 and 0.5 nm in water and ethanol, respectively. The mean size of the grains synthesized in ethanol is bigger than the size of those obtained in water, in agreement with previous reports [13].

The colloidal solutions of the Si-NPs in water and ethanol absorb in the UV-visible, as shown by Fig. 4. In both cases the absorption gradually increases as the wavelength is reduced. The absorption tail in the visible is associated with indirect transitions. For the sample grown in water, the two shoulders near 370 nm (3.3 eV) and 290 nm (4.2 eV) are associated with direct-gap absorptions, whereas those of the sample prepared in ethanol display only one shoulder, near 290 nm. Bulk

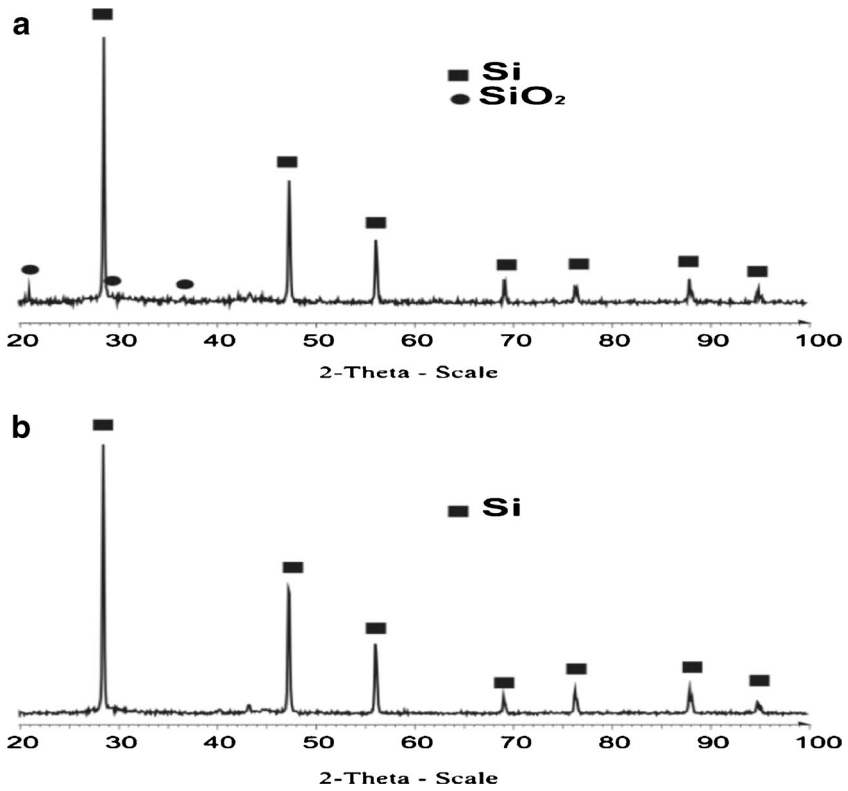

Fig. 2 Typical XRD patterns of the silicon nanopowders prepared by electrical spark discharge in **a** water and **b** ethanol

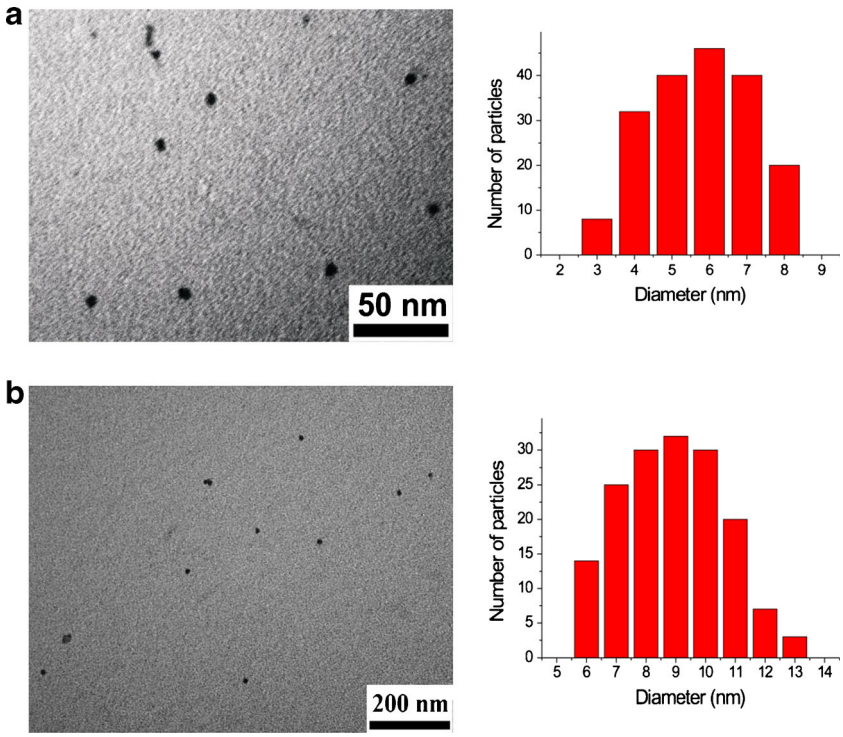

Fig. 3 (*Colored online*) TEM images and the size distribution of the Si-NPs produced by electrical-spark discharge in **a** water and **b** ethanol. The size distribution of each image is shown by the histograms on the right-hand side

silicon is characterized by indirect bandgap absorption from 1.1 to 3.4 eV and two direct-gap transitions starting around 3.2 (380) and 4.2 eV (295 nm) [20]. By comparison, the Si-NPs prepared in water and ethanol display blue-shifted absorption edges. When compared with the samples grown in ethanol, those grown in water display a more blue-shifted absorption edge. This agrees with our discussion of the TEM results, which indicated that the grain size for Si-NP production in water is smaller than for production in ethanol.

As already mentioned, Si is an indirect bandgap semiconductor. To estimate the effective gap of the Si-NPs, we have taken advantage of the following relation between the optical density and the square of photon energy [9, 10]:

$$\alpha h\nu \propto \left(h\nu - E_g\right)^2, \tag{1}$$

which shows that plots of $(\alpha h\nu)^{1/2}$ versus the photon energy ($h\nu$), where α is the measured absorption coefficient, should display linear behavior in the region of indirect transitions. The low signal-to-noise ratio in the tail region of the absorption spectrum of our samples, synthesized by submerged electrical discharge, makes the data analysis in this region rather difficult. Nevertheless, the absorption data from a few samples showed sufficiently large ratios to allow comparison with (1). Examples are shown in Fig. 4, the linear approximation being represented by a dashed line. Good agreement between the experimental data and the linear fit is observed in the energy intervals from 2.2 to 3.3 eV and from 2 to 3.5 eV for the Si-NPs synthesized in water and ethanol, respectively. We attribute the difference at lower energies to the existence of more than one absorption mechanism. It is clear that different factors can affect absorption in the Si-NPs, including the size distribution of nanoparticles, surface-state effects, and oxide-layer defects. The indirect band-gap energy for the produced Si-NPs was estimated from the intercept of the straight line with the x-axis to be about 1.5 and 1.3 eV for the samples synthesized in water and ethanol, respectively. These are wider than the gap in bulk Si, as one would expect in view of quantum confinement.

On the basis of a linear combination of atomic orbital analysis, Delerue et al. [21] have suggested the following expression relating the band gap of Si-NPs to their size d:

$$E_g = E_0 + \left(\frac{3.73}{d^{1.39}}\right), \tag{2}$$

where 3.73 and 1.39 are numbers associated with the assumed nature of the surface as well as with the symmetry and even with the size of the NPs.

From (2) and the bandgaps obtained from Fig. 4, we find that the shifts of $\Delta E = E_g - E_0$ correspond to particles diameter of 5 and 11 nm in water and ethanol, respectively. The former size is in close agreement with the TEM results, but the discrepancy for the particles prepared in ethanol is more substantial. The accuracy of the NP sizes computed from (2) can be influenced by the size distribution of particles, because the factor 3.73 and the exponent 1.39 were obtained in 23 for NPs with $d < 10$ nm and become unreliable for bigger particles.

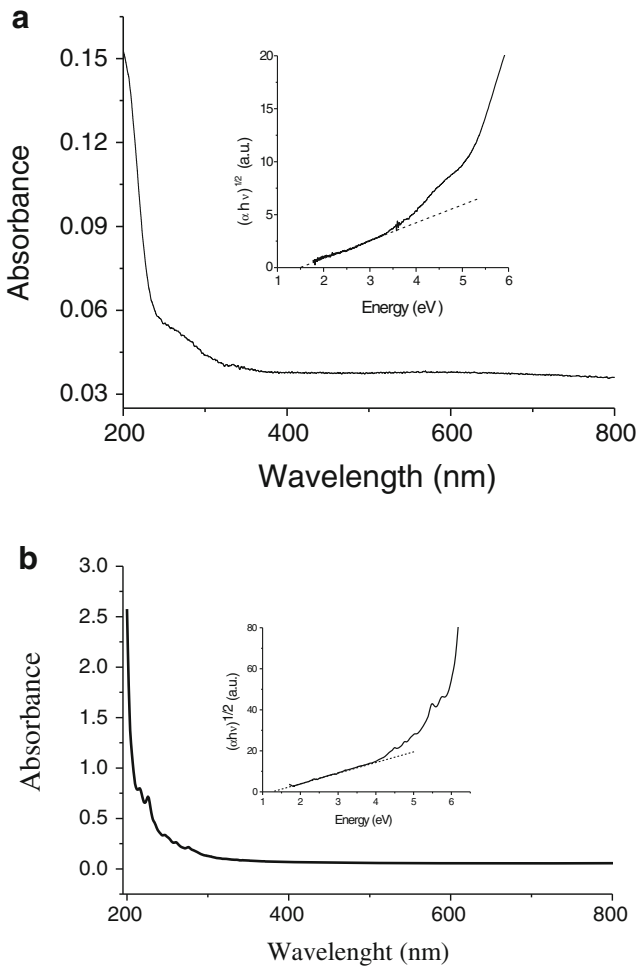

Fig. 4 Optical absorption spectra of the colloidal solution of the Si-NPs produced by spark discharge between silicon electrodes and procedure to estimate the effective bandgaps of the Si-NPs synthesized in **a** water and **b** ethanol

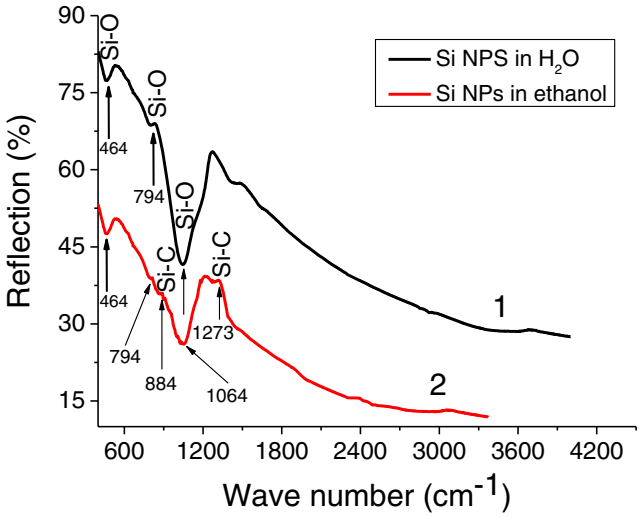

Fig. 5 (*Colored online*) FTIR spectra of the Si-NPs synthesized by electrical spark discharge of Si electrodes in water (curve 1) and ethanol (curve 2)

We have found the Si-NPs produced by electrical discharge to depend on the nature of the liquid. FTIR is a nondestructive technique yielding direct information on the compositional properties of the synthesized products. In Fig. 5, the located peaks at 1,064, 794, and 464 cm^{-1} match those of Si–O vibration bonds, suggesting that oxide layers are formed on the surface of synthesized particles. Other weak peaks in the red curve, labeled 2, are visible at 884 and 1,273 cm^{-1}, corresponding to the vibration frequency of Si–C bonds and showing that a few organic bonds may be formed on the surface of the Si-NPs synthesized in ethanol. Most probably, the nanoparticles are formed by primary nucleation of the atoms evaporated from the electrodes in the plasma plume and subsequent growth of the embryonic particles, which continues until complete consumption of all Si atoms in the immediate vicinity. When they escape from the plume into the liquid media, the particles are quickly cooled and growth is suppressed via reactive quenching with water or ethanol, which favors formation of Si–O, Si–OH, or Si–C bonds on the particle surface.

Raman spectroscopy is another powerful nondestructive tool allowing observation of quantum confinement effects in nanoscopic particles [22]. In this size range, Raman spectra evidence phonon confinement as a downshift and a broadening of the first-order Si optical peak located around 521 cm^{-1}; line-shape analysis and the so-called spatial confinement model (SCM) [20] allow quantitative assessment of the mean size. Figure 6 presents the first-order optical bands for the samples prepared in water and ethanol, compared with that for bulk Si. In our experiment, the Raman peaks for the Si-NPs synthesized in water and ethanol are blue shifted ($\Delta\omega \approx 2.5$ and 1.5 cm^{-1} for water and ethanol, respectively) relative to the peaks in the bulk Si, an indication that very small Si grains are generated in both cases. The full width at half maximum (FWHM) of the Raman peak for the Si-NPs synthesized in ethanol is larger than that coming from the NPs prepared in water, which indicates that the grain-size distribution is broader.

It is known from the literature that amorphous Si gives rise to a broad TO peak near 490 cm^{-1} [9]. The Si-NPs synthesized in our experiment show no such peak and are hence crystalline, a conclusion that agrees with the XRD results in Fig. 2.

Bulk Si shows no photoluminescence (PL) because its indirect band gap is narrow. The PL of Si nanostructures can be explained by a number of effects. As the diameter shrinks to several nanometers, quantum confinement may efficiently allow light emission. Since the bulk excitonic radius for Si is about 4 nm, emission through direct electron-hole recombination across the Γ-Γ direct bandgap is expected for nanocrystals that are smaller than this size [20]. It has been also reported that the surface states, defects, or impurities can act as radiative centers and hence play significant roles in luminescence [21, 23, 24], although the origin of photoluminescence is still a subject of debate.

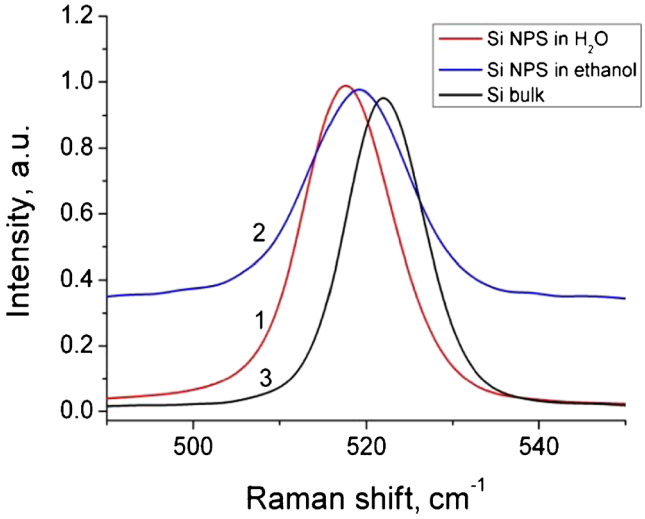

Fig. 6 (*Colored online*) Raman scattering spectra of the Si-NPs synthesized by spark discharge between Si electrodes in water (curve 1) and ethanol (curve 2), compared to bulk silicon (curve 3)

Figure 7 shows the PL spectrum under 270 nm wavelength excitation at room temperature for both Si colloidal solutions. For clarity, the PL intensity of the colloidal solution prepared in ethanol is multiplied by a factor 10. The PL of the Si-NPs generated in water exhibits a prominent emission band in the violet-blue range with a double peak around 417 and 439 nm, while that in ethanol shows a blue-green emission centered at 463 nm. This observation is in agreement with previous work on the luminescence of Si-NPs [13, 25–27]. In the case of the colloidal solution prepared in water, the mean size of the generated Si-NPs is about 5 nm as shown by the particle-size histogram in Fig. 3.

Account taken of the 4 nm exciton Bohr radius for Si, the intense PL of the Si-NPs is assumed to arise from carrier recombination in a confinement regime. Nevertheless the observed violet-blue light emission in the PL spectrum cannot be simply attributed to quantum confinement of the NPs with

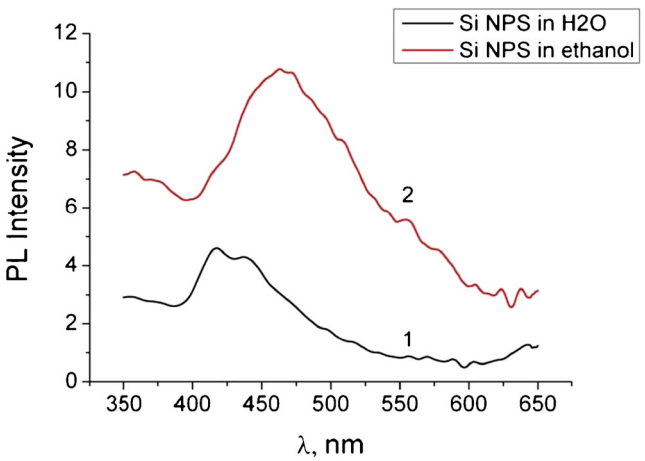

Fig. 7 (*Colored online*) Photoluminescence spectra of the Si-NPs colloidal solutions synthesized by electrical spark discharge between Si electrodes in water (curve 1) and ethanol (curve 2)

diameters in the 3–8 nm range, because only a few particles in this size range were detected in the TEM images. Therefore radiative recombination via the defect centers on the surface oxide layer of the Si-NPs or at the interface between the Si nanocrystal and Si oxide layer is the most likely mechanism for the observed blue PL. Indeed, according to the FTIR spectra, these Si-NPs are covered with oxygen (oxide). Oxide-related defects may well be formed within the surface oxide layer of the Si-NPs, which would act as radiative centers for electron-hole recombination [21, 23]. Dangling bonds on the surface give rise to various surface states deep in the energy gap. As the electron-hole pairs are generated, most likely through photoexcitation in the crystalline Si cores, light emission is observed after recombination of electrons and holes at the luminescent centers at the core-oxide layer interface or in the oxide surface.

The Si-NPs colloidal solution prepared in ethanol exhibits a red-shifted PL emission with a peak maximum at 463 nm and a decreased intensity relative to the observed PL of those prepared in water. Moreover, the PL maximum is shifted to larger wavelengths, indicating rather large Si-NPs. The PL peak of Si-NPs is red shifted as the nanoparticle mean size increases due to quantum confinement, an effect that occurs when the nanoparticle size is comparable to the Bohr radius of the exciton [28]. In the case of the Si-NPs synthesized in ethanol, the nanoparticle mean size is around 9 nm, significantly larger than the exciton Bohr radius. The luminescence of the Si-NPs is therefore in a weak-confinement regime, with a lower bandgap and, therefore, an emission red shift [25]. We believe that Si–C bonds related defects on the surface of these nanoparticles, as well as the bigger size of the latter, block the PL process detected in the samples prepared in ethanol. Nonetheless, more detailed excitation-spectrum studies are necessary to validate this explanation.

4 Conclusion

The electrical-discharge method in a liquid environment is a simple, effective technique yielding large amounts of nanoparticles in the form of a suspension in the liquid. The freedoms to adjust discharge parameters and to choose the liquid give some control over the nanoparticle properties. The absorption spectra of the NPs prepared via electrical spark discharge between Si electrodes show that the bandgaps of the silicon colloidal solution in water and ethanol are close to 1.5 and 1.3 eV, respectively. The synthesis in ethanol yielded slightly oxidized Si-NPs, as inferred from XRD, FTIR, and Raman experiments. The luminescence properties of the particles showed that the oxidation differs from that in Si-NPs obtained in water. We have also found that elementary carbon results from the partial decomposition of ethanol during the electrical discharge, since FTIR identified a Si–C phase in the

synthesized particles, the proportion of Si–C being nonetheless too low to be detected by XRD. The most likely mechanism for the observed PL of the nanoparticles grown in water is radiative recombination at the defect centers in the surface oxide layer. EDL allowed us to produce the Si-NPs with average diameters of 5 and 9 nm in water and ethanol, respectively. We conclude that the nanoparticles synthesized in water (<10 nm) are more suitable candidate for bio-imaging applications.

Acknowledgments This work was financially supported by the National Academy of Sciences of Belarus (Grant No. 2.6.01) and the Belarusian Foundation for Fundamental Researches (Grant No. F12MC-006). The authors would like to thank E.I. Mosunov for the XRD measurements, A.P. Stupak for the photoluminescence investigations, A.G. Karosa for the Raman and FTIR measurements, and K.V. Skrockaya for assistance with the TEM measurements.

References

1. K.Y. Cheng, R. Anthony, U.R. Kortshagen, R.J. Holmes, Nano Lett. **11**(5), 1952–1956 (2011)
2. L. Pavesi, L.D. Negro, C. Mazzoleni, G. Franzo, F. Priolo, Nature **408**(6811), 440–444 (2000)
3. V. Svrcek, D. Mariotti, T. Nagai, Y. Shibata, I. Turkevych, M. Kondo, J. Phys. Chem. C **115**(120), 5084–5093 (2011)
4. F. Erogbogbo, K.T. Yong, I. Roy, G.X. Xu, P.N. Prasad, M.T. Swihart, ACS Nano **2**(5), 873–878 (2008)
5. N.H. Alsharif, C.E.M. Berger, S.S. Varanasi, Y. Chao, B.R. Horrocks, H.K. Datta, Small **5**(2), 221–228 (2009)
6. F. Priolo, G. Franzo, D. Pacifici, V. Vinciguerra, J. Appl. Phys. **89**, 264 (2001)
7. C. Grigoriu, Y. Kuroki, I. Nicolae, X. Zhu, M. Hirai, H. Suematsu, M. Takata, K. Yatsui, J. Optoelectron. Adv. Mater. **7**, 2979 (2005)
8. K. Watanabe, K. Sawada, M. Koshiba, M. Fuji, S. Hayashi, Appl. Surf. Sci. **635**, 197–198 (2002)
9. N.G. Semaltianos, S. Logothetidis, W. Perrie, S. Romani, R.J. Potter, S.P. Edwardson, J. Nanopart. Res. (2009). doi:10.1007/s11051-009-9625-y
10. S. Yang, W. Cai, H. Zeng, Z. Li, J. Appl. Phys. **104**, 023516–1 (2008)
11. M. Rosso, E. Spruigt, Z. Popovic, K. Overgaag, B. Van, B. Grandidier, D. Vanmaekelbergh, D. Dominguez, L.D. Cola, H. Zuilhof, J. Mater. Chem. **19**(33), 5926–5933 (2009)
12. X. Zhang, D. Neiner, S. Wang, A.V. Louie, S.M. Kauzlarich, Nanotechnology **18**(9), 095601 (2007)
13. S. Yang, W. Cai, H. Zhang, X. Xu, H. Zeng, J. Phys. Chem. C **113**, 19091 (2009)
14. R. Intartaglia, K. Bagga, F. Brandi, G. Das, A. Genovese, E. Di Fabrizio, A. Diaspro, J. Phys. Chem. C **115**, 5102 (2011)
15. W.G. Graham, K.R. Stalder, J. Appl. Phys. **44**, 174037 (2011)
16. N. Parkansky, B. Alterkop, R.L. Boxman, S. Goldsmith, Z. Barkay, Y. Lereah, Powder Technol. **150**, 36 (2005)
17. V.S. Burakov, N.A. Savastenko, N.V. Tarasenko, E.A. Nevar, J. Appl. Spectrosc. **75**, 114 (2008)
18. V.S. Burakov, E.A. Nevar, M.I. Nedel'ko, N.A. Savastenko, N.V. Tarasenko, J. Appl. Spectrosc. **76**, 856 (2009)
19. A. V. Kabashin, M. Meunier, Elsevier: Oxford (2006)
20. J.P. Wilcoxon, G.A. Samara, P.N. Provencio, J. Phys. Rev. B **60**(4), 2704–2714 (1999)
21. C. Delerue, G. Allan, M. Lannoo, J. Phys. Rev. B **48**, 11024 (1993)
22. M. Kobayashi, S. Man Liu, S. Sato, H. Yao, K. Kimura, Jpn. J. Appl. Phys. **8A**, 6146 (2006)
23. V. Paillard, P. Puech, M.A. Laguna, A. Carles, B. Kohn, J. Appl. Phys. **86**, 1921 (1999)
24. H. Richter, Z.P. Wang, L. Ley, Solid State Common. **39**, 625 (1981)
25. M.R. Vasik, E. Spruijt, Z. Popovik, K. Overgaag, B.V. Lagen, B. Grandidier, D. Vanmaekelbergh, D.D. Gutierrez, L.D. Kola, H. Zuilhof, J. Mater. Chem. **19**(33), 5926–5923 (2009)
26. G. Belomoin, J. Therrien, A. Smith, S. Rao, R. Twesten, S. Chaieb, M.H. Nayfeh, Appl. Phys. Lett. **80**(5), 841–843 (2002)
27. T. Uchino, N. Kurumoto, N. Sagawa, J. Phys. Rev. B **73**, 233203 (2006)
28. S. Yang, W. Li, B. Cao, H. Zeng, W. Cai, J. Phys. Chem. C **115**(43), 21056–21062 (2011)